

## Chapter 4

# Dynamics of the 50 Ma Plate Reorganization

### 4.1 Abstract

The cause of relatively rapid plate reorganizations in the past, including the change in the direction of the Pacific plate at  $\sim 50$  Ma, is not well known. Whether such changes are driven by mantle or plate processes is the subject of ongoing discussion. We use high-resolution instantaneous dynamic mantle convection models capable of resolving plate boundaries at a fine scale,  $\sim 1$  km, to study the reorganization occurring around 50 Ma. This event is commonly associated with a swerve in direction of Pacific plate motion and major tectonic events in the Pacific region, including initiation of Izu-Bonin-Marianas and Tonga-Kermadec subduction. Slab break-off at the East Asian subduction zone, related to arrival of the Izanagi-Pacific spreading ridge at the trench, as well as plate motion changes in the Atlantic and Indian oceans expressed by fracture zone bends, may also be related to the reorganization. The plate boundaries in our models are derived from global plate reconstructions, and the thermal structure is obtained from time-dependent convection models with a resolution of  $\sim 40$  km. A composite viscosity including non-Newtonian viscosity and yielding allows for localization of deformation in the plates, bending slabs, and upper mantle. The resulting models are validated

against the inferred plate motions at 55 and 45 Ma. We further compare model outcomes at these times in terms of (changes in) surface velocities, intraplate deformation, state of stress, and mantle flow. We concentrate on the Pacific plate as it was subject to a major change in motion during the reorganization, while focusing on the initiation and cessation of subduction in the western Pacific.

## 4.2 Introduction

Reconstructions of past plate motions are typically created using a wide variety of constraints, including paleomagnetic data (e.g. apparent polar wander paths), geologic restorations of conjugate continental margins, volcanic records for onset of new subduction zones, and marine surveys of magnetic anomalies and seafloor bathymetry, especially fracture zone orientations.

Although relatively detailed plate tectonic evolution can be reconstructed back to  $\sim 250$  Ma (*Torsvik et al., 2010; Seton et al., 2012*), the force balance associated with this evolution is poorly understood. A crucial example is the enigma of rapid plate reorganizations. During these events, plate motions significantly changed orientation, while plate boundaries were formed or destroyed all within a few millions of years. Several such plate reorganizations have been inferred, including ones at around 100 Ma, 50 Ma, and 6 Ma (*Wessel et al., 2006; Austermann et al., 2011*). The cause of these reorganizations is subject to significant discussion, and the main topic of this chapter.

We focus on the reorganization at  $\sim 50$  Ma, as there is a relative abundance of available observations and limited error in reconstructions compared to older events. The best-known manifestation of this event is the bend in the Hawaiian-Emperor chain (HEB), dated between 47 and 50 Ma (*Sharp and Clague, 2006; Tarduno et al., 2009*), and thought to represent

a significant change in the absolute motion of the Pacific plate in both fixed and moving hotspot reference frames. The initiation of the Izu-Bonin-Marianas (IBM) and Tonga-Kermadec subduction zones around 50 Ma is a second component of the plate tectonic puzzle (*Stern and Bloomer, 1992; Gurnis et al., 2004*). Other concurrent phenomena include the South Pacific triple junction reorganization and the collision of the Indian and Eurasian continents (*Wessel et al., 2006; Cande and Stegman, 2011*).

The initiation of subduction may have been an essential part in the chain of events during the 50 Ma reorganization, likely caused by, as well as reinforcing, the change in motion of the Pacific plate (e.g., *Gurnis et al. (2004)*). *Whittaker et al. (2007)* propose that the completion of subduction of the Izanagi-Pacific Ridge (IPR) resulted in massive slab break-off along the Japanese trench, changing the forces on the Pacific plate from ridge-push to slab-pull and initiating a rotation of plate velocity from northwest to west around 53 Ma. This change in Pacific plate motion caused cessation of Tasman Sea spreading at  $\sim 52$  Ma. Increased slab pull north of Australia due to westerly progression of the subducting Wharton Basin ridge (to the northwest of Australia) changed the absolute plate motions of Australia from northwest to north, and caused faster spreading between Australia and Antarctica. The combination of Australia and Pacific plate motion changes between 53 and 50 Ma could then nucleate the initiation of the IBM and Tonga-Kermadec subduction zones, further increasing the westward rotation of the Pacific plate. *Whittaker et al. (2007)* additionally suggest that the observed subsequent slowdown of sub-Pacific mantle flow at 47 Ma (*Tarduno et al., 2003*) may have been caused by the progressive impediment of lateral sub-Pacific flow by the descending slabs. This constitutes a “top-down” view, where plate motions steer the reorganization and govern mantle flow (e.g., *Anderson (2001)*).

However, several studies have at least partly attributed the HEB to southward movement

of the underlying Hawaiian hotspot prior to  $\sim 50$  Ma (*Steinberger et al.*, 2004; *Tarduno et al.*, 2003). Temporary pinning of the plume by a nearby ridge could cause significant hotspot motion (*Tarduno et al.*, 2009). Mantle plumes may have an important effect on the driving of plate motions, specifically the arrival of a plume head below the lithosphere together with the associated lateral asthenospheric flow (*Cande and Stegman*, 2011; *van Hinsbergen et al.*, 2011). These observations and inferences are consistent with the “bottom-up” view where mantle flow drives plate motion (e.g. *King et al.* (2002)).

Whether the top-down or bottom-up view best represents the force balance of the Earth’s convective system has implications for the coupling between mantle flow and plate motions (*Crowley and O’Connell*, 2012). Numerical convection models at the time of plate reorganizations that include both mantle and plates provide a way to obtain greater insight into this force balance. *Richards and Lithgow-Bertelloni* (1996) tested the hypothesis that the collision between India and Eurasia gave rise to the HEB by combining the Indian and Eurasian plates into one. In these models, no appreciable effect on the motion of the Pacific plate was found, and no convergence arises between the Pacific and Australian boundaries. Instead, the authors speculate that the HEB is caused by the sudden change from transverse motion to subduction along preexisting transform faults in the western Pacific. In a more extensive study, *Lithgow-Bertelloni and Richards* (1998) investigated the kinematics of the last 120 My of plate motions and dynamics of Cenozoic motions by means of a self-consistent model of plate motions. This model was constructed from a simplified subduction history, for which the induced plate motions for each stage of the Cenozoic was approximately reproduced, except for the stage after the HEB. The study shows that the main plate-driving forces arise from subducted slabs ( $> 90\%$ , predominantly in the lower mantle), with forces due to lithospheric effects such as oceanic plate thickening providing a minor component ( $< 10\%$ ). However, sudden plate mo-

tion changes defined by stage boundaries, such as the westward rotation of the Pacific implied by the HEB, remain unexplained. *Conrad and Lithgow-Bertelloni (2004)* further constrain the relative importance of slab suction and slab pull by comparing Cenozoic plate motions to model predictions that include viscous mantle flow and a proxy for slab strength. Slab pull from upper mantle slabs combined with slab suction from lower mantle slabs reproduce the observation that subducting plates currently move  $\sim 4$  times faster than nonsubducting plates, and the temporal evolution of plate motions is explained through increase of slab length with time. Although the speedup of the Pacific during the latter half of the Cenozoic is predicted, the rapid northerly to westerly change in Pacific plate motion direction indicated by the HEB is not. Instead, the shift in plate motion direction gradually evolves during the entire Cenozoic.

A different approach is used by *Faccenna et al. (2012)*, where the role of slab pull acting on the Pacific plate is analyzed during its early Tertiary change in motion. In this study, slab pull forces are estimated by integrating the negative buoyancy of a 700 km long slab along subduction boundaries. The torques predicted from this simple slab pull model match the directions of Pacific plate Euler vectors during the Tertiary fairly well, and the authors suggest that the change of the Pacific motion at  $\sim 50\text{--}40$  Ma is driven by the onset of the Izu-Bonin-Mariana system and, soon afterwards, by the Tonga-Kermadec subduction zones.

The limitation in these previous studies is that the flow models, although capable of predicting general plate motions, could not resolve key features such as plate boundaries and localized deformation in subducting plates. In this paper, we use the finite element code *Rhea* to compute global dynamic convection models with plates. This code utilizes adaptive mesh refinement (AMR) (e.g., *Burstedde et al. (2008a)*). AMR ensures a high resolution in areas of the model domain that have high gradients in viscosity and temperature, while allowing a lower resolution elsewhere. This technique reduces the total number of elements in a

numerical mesh, rendering global convection computations with well-resolved plate boundaries computationally feasible (Stadler *et al.*, 2010; Alisic *et al.*, 2010, 2012); see Chapter 3. We study the 50 Ma plate reorganization through the use of use high-resolution dynamic mantle convection models capable of resolving plate boundaries at a fine scale, mitigating the severe limitations of previous flow models. A composite viscosity, including a non-Newtonian component as well as yielding, allows for localization of deformation in the plates and upper mantle. These instantaneous models are validated by reproducing inferred plate motions at 55 and 45 Ma. We then compare model outcomes at 55 and 45 Ma in terms of (changes in) intraplate deformation, state of stress, and mantle flow.

### 4.3 Methods

We compute instantaneous dynamic global models of mantle convection with plates at 55 and 45 Ma before and after the plate reorganization. These models are computed using the equations, preconditioning, solver, and meshing techniques described in detail in Section 3.3. The utilization of adaptive mesh refinement allows for resolution of plate boundaries and other strongly deforming areas at a fine scale. A major difference with the present-day models presented earlier is the manner in which the model input is assembled, as we now depend on reconstructions of plates and mantle structure in the geologic past for the locations of plate boundaries, lithospheric thickness, slab morphology, and transition zone and lower mantle structure.

The software `GPlates` was used to obtain plate boundaries at 55 and 45 Ma (Boyden *et al.*, 2011; Gurnis *et al.*, 2012b). The changes in plate motions and the nature of plate boundaries associated with the plate reorganization around 50 Ma described in the introduc-

tion are represented in the `GPlates` reconstructions (see Figures 4.1 and 4.2). On the northwest boundary of the Pacific plate, the subduction of the Izanagi-Pacific Ridge (IPR) occurs between 60 and 55 Ma (Figure 4.1a–b). To the west of the southwestern corner of the Pacific plate, the Tasman Sea spreading ceases between 55 and 50 Ma (Figure 4.1b, d). Between 50 and 45 Ma, the Pacific plate motion rotates from northwest to west, and the spreading between the Australia and Antarctica plates increases significantly (Figure 4.1d–e). In the same time period, subduction is initiated in the Tonga-Kermadec (TK) and the Izu-Bonin-Marianas (IBM) subduction zones on the western boundary of the Pacific plate (Figure 4.2d–e).

Without tomography models to infer mantle structure, we rely on predictions from time-dependent convection models. It is possible to infer mantle structure from tomography for past times with an inverse convection model (see e.g. *Liu and Gurnis (2008)*), but with current methods this would result in broad and smooth representations of slabs, and well-defined slabs are essential. The time-dependent models are computed with `CitcomS` (*Tan et al., 2006*), and are based on the same `GPlates` line data, plate rotations, and age grids, but at a lower resolution making time stepping from 250 Ma computationally feasible. The `CitcomS` mesh has a lateral mesh size of  $\sim 40$  km. The reconstructed age grids shown in Figure 4.1e–f and 4.2e–f are used to define the thermal structure of the lithosphere. In the top 350 km of the mantle, slabs associated with reconstructed subduction zones are assimilated with a specified age and thickness, a  $45^\circ$  slab dip with a radius of curvature of 200 km (*Gurnis et al., 2012a*). These slabs are then advected using reconstructed plate motions as surface velocity boundary conditions and the overall computed convective flow, such that an estimate of overall mantle structure can be obtained at any intermediate geologic time since 250 Ma. This low-resolution temperature field at 55 and 45 Ma is used in the construction of the `Rhea` temperature field, replacing the tomography and other geophysical constraints used in the present-day models

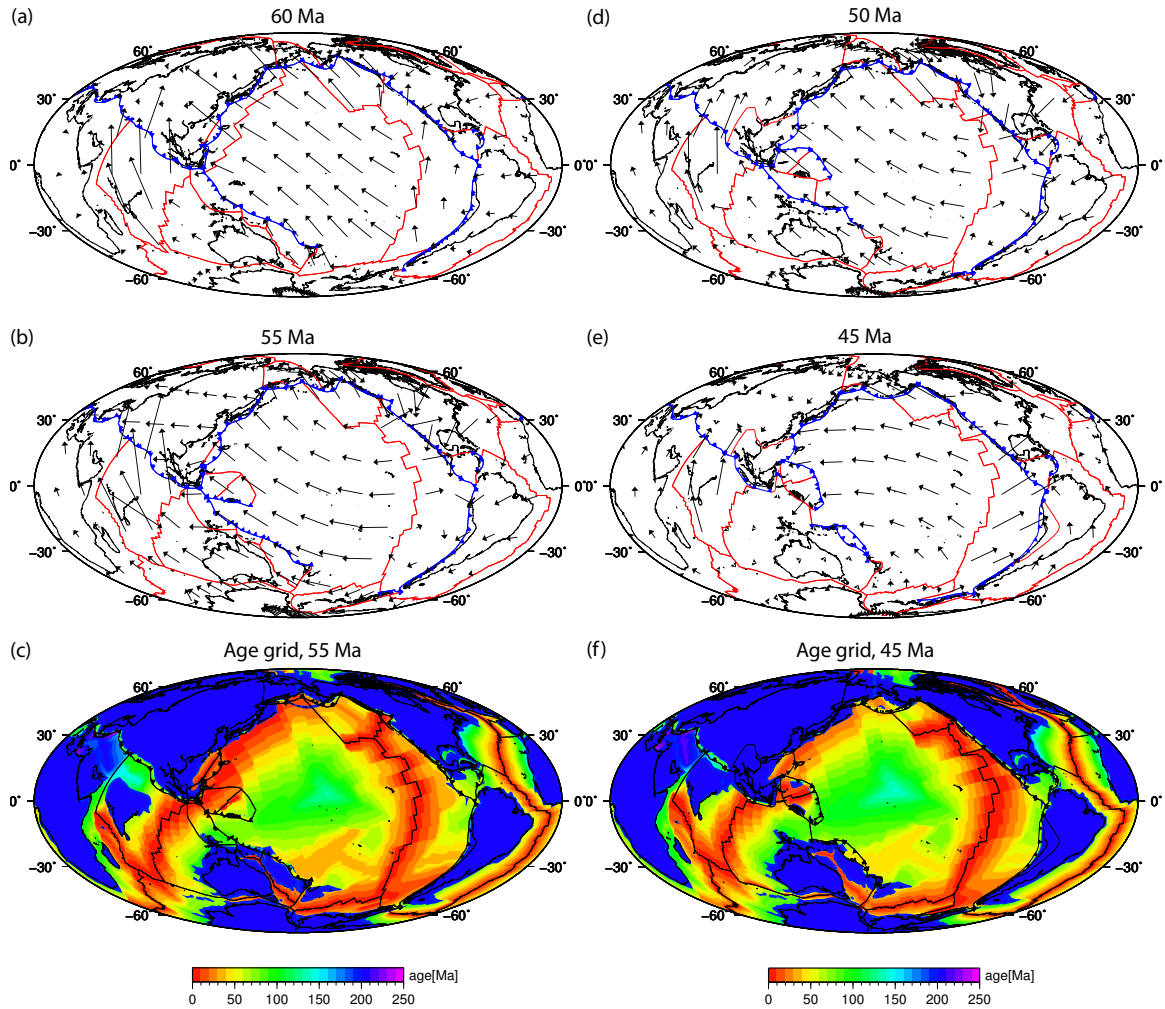


Figure 4.1. (a) GPlates reconstruction of global plate motions at 60 Ma; (b) 55 Ma; (c) Reconstructed age grid at 55 Ma; (d) Reconstructed plate motions at 50 Ma; (e) 45 Ma; (f) Reconstructed age grid at 45 Ma.

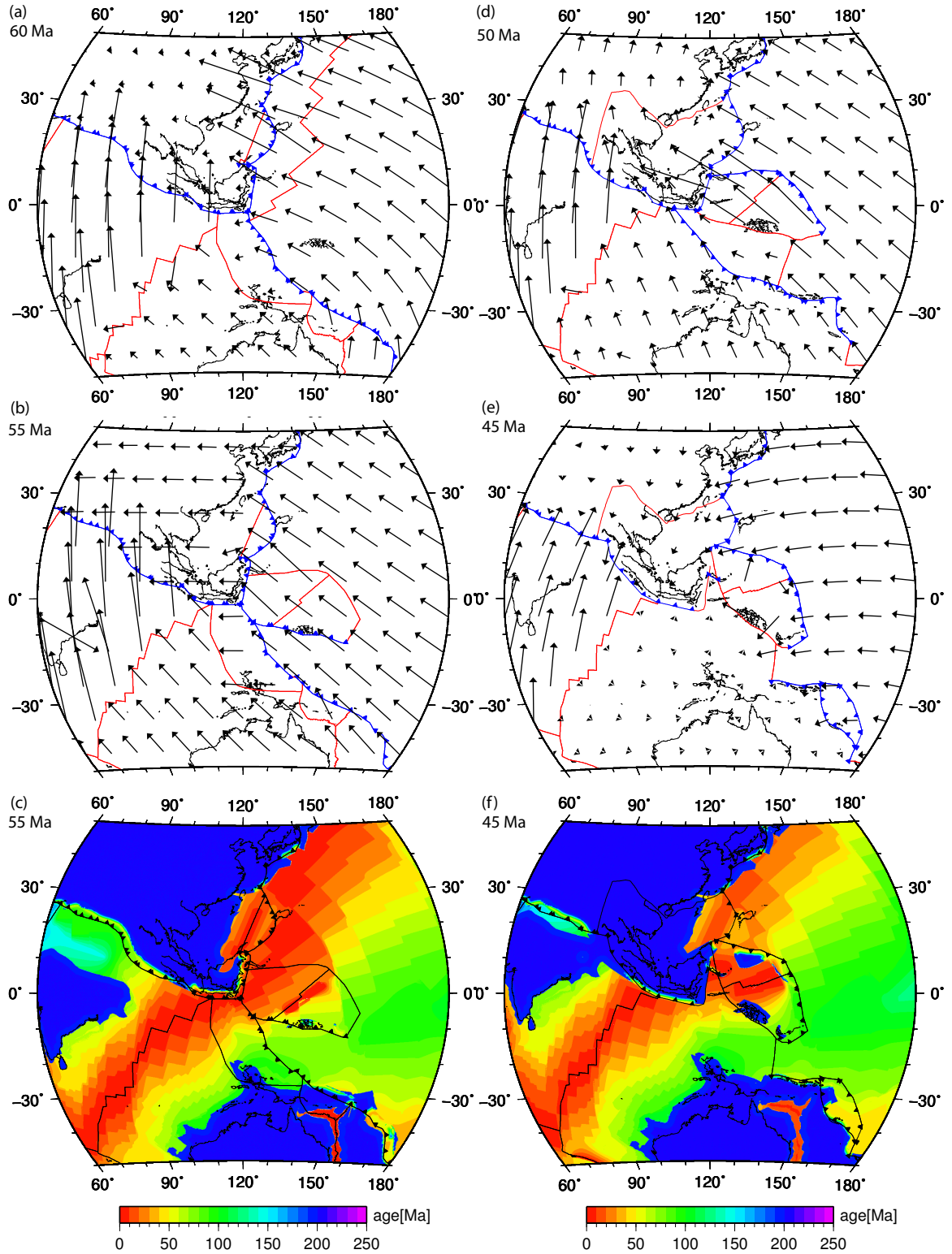


Figure 4.2. (a) GPplates reconstruction of plate motions in the western Pacific at 60 Ma; (b) 55 Ma; (c) Reconstructed age grid at 55 Ma; (d) Reconstructed plate motions at 50 Ma; (e) 45 Ma; (f) Reconstructed age grid at 45 Ma.

(model “BO4” in *Bower et al. (2012)*).

It is essential for the dynamic models with plate motions that slabs are sharply resolved, so that the slabs act as stress guides (see Section 3.2.2). To ensure that slabs retain their sharpness in the top 350 km of the mantle, we re-assimilate the slabs in this depth interval at `Rhea` mesh levels (which are different from the `CitcomS` levels) and incorporate this into the overall `Rhea` temperature field, together with the low-resolution `CitcomS` mantle structure and the lithospheric structure from the reconstructed age grids. The resulting mesh in the `Rhea` models has a resolution of  $\sim 1$  km around plate boundaries, and 2–10 km elsewhere in the plates and slabs. In other areas of the mantle with smaller temperature and viscosity gradients away from slabs, the resolution is 80–150 km.

We use the composite rheology law described in Section 3.3.2, combining linear diffusion creep, nonlinear dislocation creep, and yielding. The strain rate dependent components (dislocation creep and yielding) allow for localized weakening, which is crucial to allow otherwise stiff plates to bend in subduction zones. We assume the same bulk rheology in the past as today. Therefore, we use the parameter values that provide the best fit to the various constraints on present-day models explored in Section 3.4, namely a stress exponent  $n = 3.0$  and yield stress  $\sigma_y = 100$  MPa. The geological boundaries derived from paleo plate reconstructions are used to define weak zones that effectively decouple the plates, by means of a pre-exponent to the viscosity of  $10^{-5}$  (see Section 3.3.2). The time-dependent model used to derive the mantle structure has a significant fraction of high-viscosity slab remnants accumulated in the lower mantle. Therefore, we use a smaller grain size in the lower mantle compared to Chapter 3 ( $70 \times 10^3 \mu\text{m}$  instead of  $100 \times 10^3 \mu\text{m}$ ), to compensate for the increase in bulk lower mantle viscosity with respect to a smoother lower mantle structure from tomography.

Model outcomes are velocities at the surface and in the interior of the mantle, viscosity,

strain rate, and state of stress. The models at 55 and 45 Ma are validated by comparing model surface velocities to reconstructed plate motions. We then study changes in surface strain rate, viscosity, and state of stress between the 55 and 45 Ma models. In addition, viscosity, velocity, and the state of stress in several cross-sections around the Pacific ocean are compared. We also study lateral flow patterns in the mantle for clues of causes and effects of the plate reorganization at around 50 Ma.

## **4.4 Results**

### **4.4.1 Model Viscosity**

The use of time dependent models to create mantle structure results in features that are significantly sharper compared to structures derived from tomography, especially in the lower mantle (see Chapter 3). The advected slabs and their remnants have a considerable lifespan as they accumulate in the lower mantle (Figure 4.3b–c). These high-viscosity features are relatively stable; we do not see significant changes in their position or shape between 55 Ma and 45 Ma.

### **4.4.2 Plate Motions**

A first requirement of a dynamic convection model with plates is that deformation primarily takes place at plate boundaries rather than within plate interiors. The models at 55 Ma and 45 Ma indeed display this localized deformation, illustrated by high strain rates and low viscosities at the plate boundaries, while plate interiors are generally strong with high viscosities and low strain rates (Figures 4.4a–d and 4.5a–d). One exception can be seen at the western edge of the Pacific plate, where the subduction of the Pacific-Izanagi Ridge had just completed

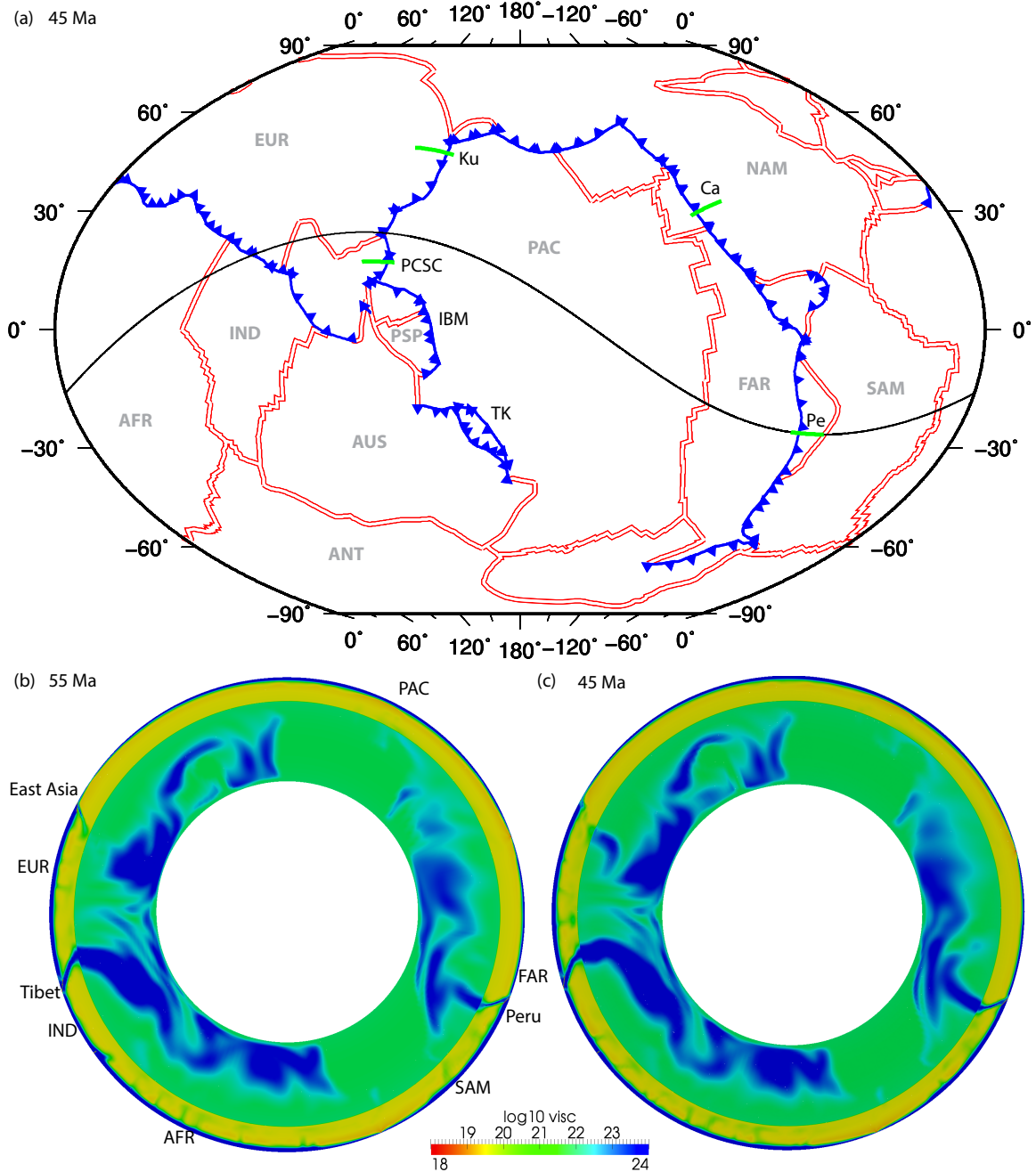


Figure 4.3. (a) Map with locations of the annulus shown in panels (b) and (c) (black), and the cross-sections of Figures 4.8 and 4.9 (green). Note that the plate boundaries are plotted at their 45 Ma configuration to show the newly formed subduction zones. (b) Global cross-section through model viscosity at 55 Ma; (c) 45 Ma. Plate abbreviations: AFR: Africa; ANT: Antarctica; AUS: Australia; EUR: Eurasia; FAR: Farallon; IND: India; NAM: North America; PAC: Pacific; PSP: Philippine Sea Plate; SAM: South America. Cross-section abbreviations: Ca: California; Ku: Kurile; PCSC: Proto-South China Sea; Pe: Peru. Subduction zone abbreviations: IBM: Izu-Bonin-Marianas; TK: Tonga-Kermadec.

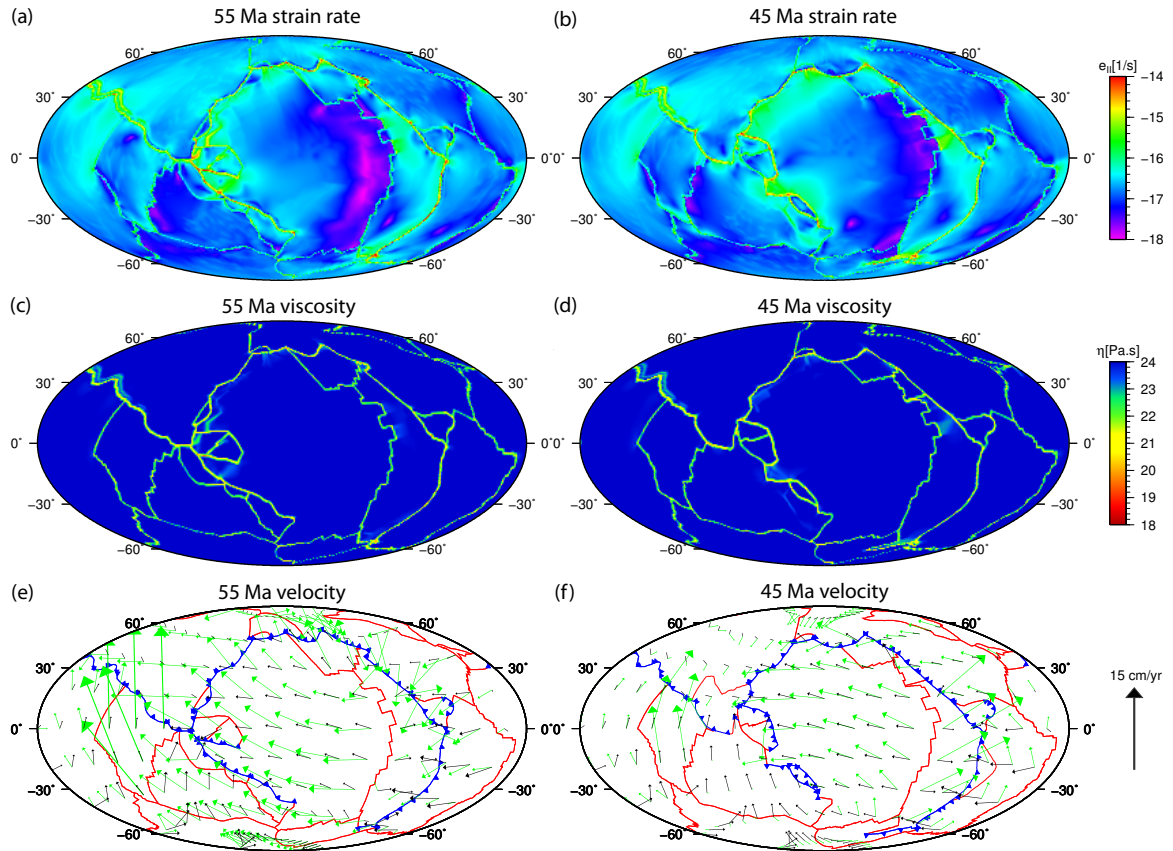


Figure 4.4. Map view of modeled surface quantities; global view centered on the Pacific at 55 Ma (left) and 45 Ma (right). (a)–(b): Second invariant of the strain rate; (c)–(d): Viscosity; (e)–(f): Velocities from the dynamic model (black) and from plate reconstructions (green). No line data is plotted in the viscosity and strain rate panels.

by 55 Ma. Young and therefore thin oceanic lithosphere still remains (see Figures 4.1e and 4.2e), which is easier to deform than the surrounding thicker lithosphere on the Pacific plate. Another narrow band of deformation is present to the south of this area, in the Pacific plate just east of Australia and north of the Tasman Sea Ridge. Interestingly, this is at the location where later an inferred boundary between the Pacific and the Indo-Australia plate has developed at 45 Ma (Figure 4.2f).

The model surface velocities are compared with velocities derived from *GPlates* paleo plate reconstructions (Figures 4.4e–f and 4.5e–f). The fit in plate motions is poor. Most plates are moving too slow, especially the ones that have subducting slabs attached to them, such

as the Pacific, Australia, India, and Kula plates. The Pacific plate is moving almost due west in the 55 Ma model, lacking a northward component. The Australia plate is moving to the northeast instead of the northwest. At 45 Ma, the Pacific plate continues moving westward in the dynamic model without much change, only its southern section shows a decrease in northward motion. The Australia plate now moves more to the north, but the other plates have not significantly changed direction. The lack in plate motion change could be linked to the highly stationary lower mantle slab remnants, which we will explore further. An exception is the fast clockwise rotation of the Philippine Sea Plate between 55 and 45 Ma (center of Figure 4.5e–f), which is also observed in the plate motion reconstructions.

An important characteristic of global plate motions is the net rotation of the surface, which describes the rotation of the entire surface with respect to the deep mantle. Estimates of this net rotation for the past 150 Ma by *Torsvik et al. (2010)* are significantly smaller than in the *GPlates* reconstruction, even when the net rotation from the plate reconstruction is averaged into the same intervals as used in the estimate by *Torsvik et al. (2010)*. (Figure 4.6). The slow and relatively unchanging plate motion in the dynamic plate motion models is reflected in the net surface rotation, which, approximately constant at  $0.11^\circ/\text{My}$  in a westward orientation (dominated by the motion of the Pacific plate), is significantly smaller than both the *GPlates* prediction and the prediction by *Torsvik et al. (2010)* at 55 Ma (respectively  $0.52$  and  $0.33^\circ/\text{My}$ ). The *GPlates* model as well as the model by *Torsvik et al. (2010)* show a strong decrease in net rotation at 45 Ma compared to 55 Ma:  $0.20^\circ/\text{My}$  and  $0.08^\circ/\text{My}$ , respectively. The net rotation in the dynamic model, still at  $0.11^\circ/\text{My}$ , is more similar to these predictions at this time.

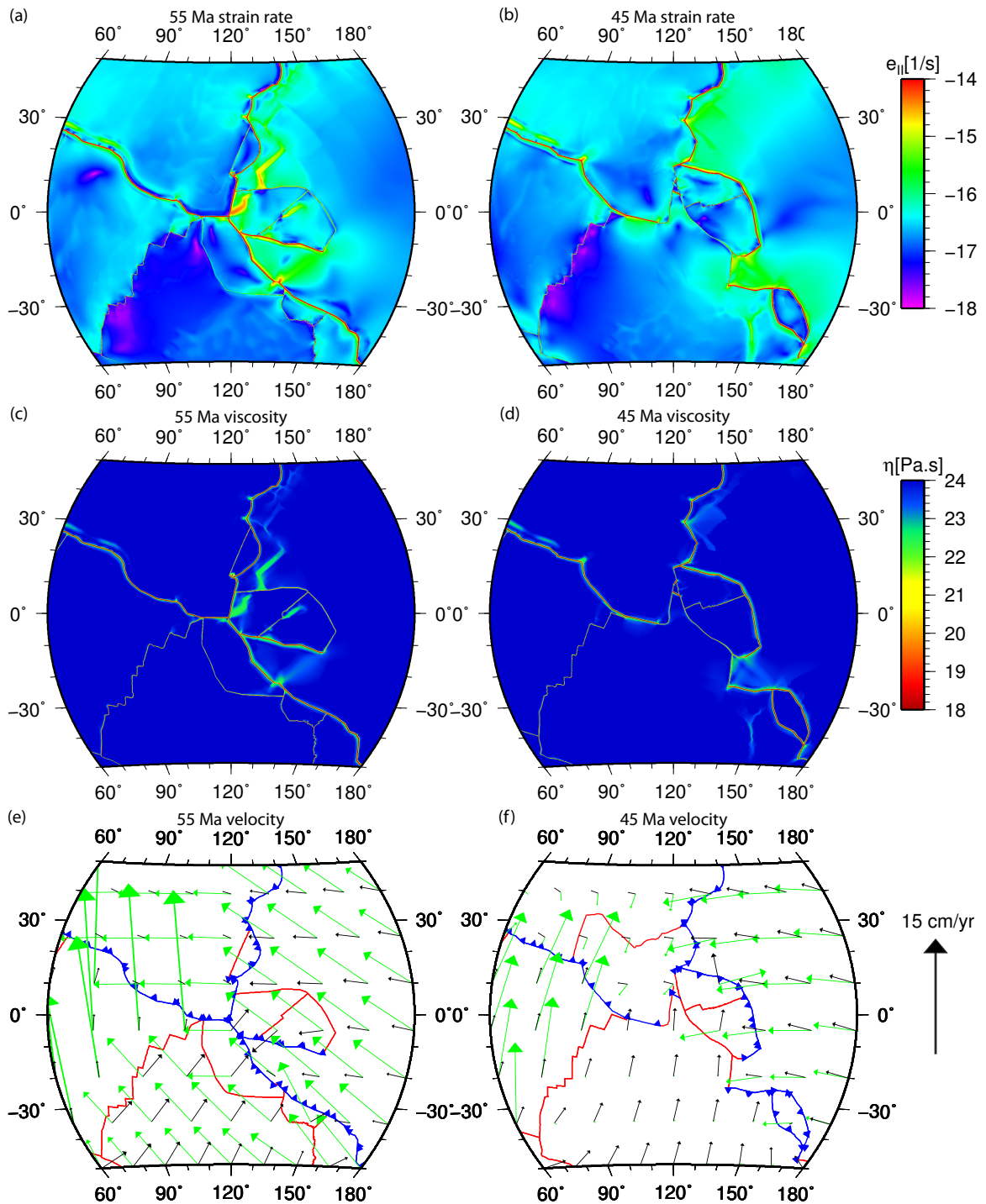


Figure 4.5. Map view of modeled surface quantities; zoom-in on the western Pacific at 55 Ma (left) and 45 Ma (right). (a)–(b): Second invariant of the strain rate; (c)–(d): Viscosity; (e)–(f): Velocities from the dynamic model (black) and from plate reconstructions (green). No line data is plotted in the viscosity and strain rate panels.

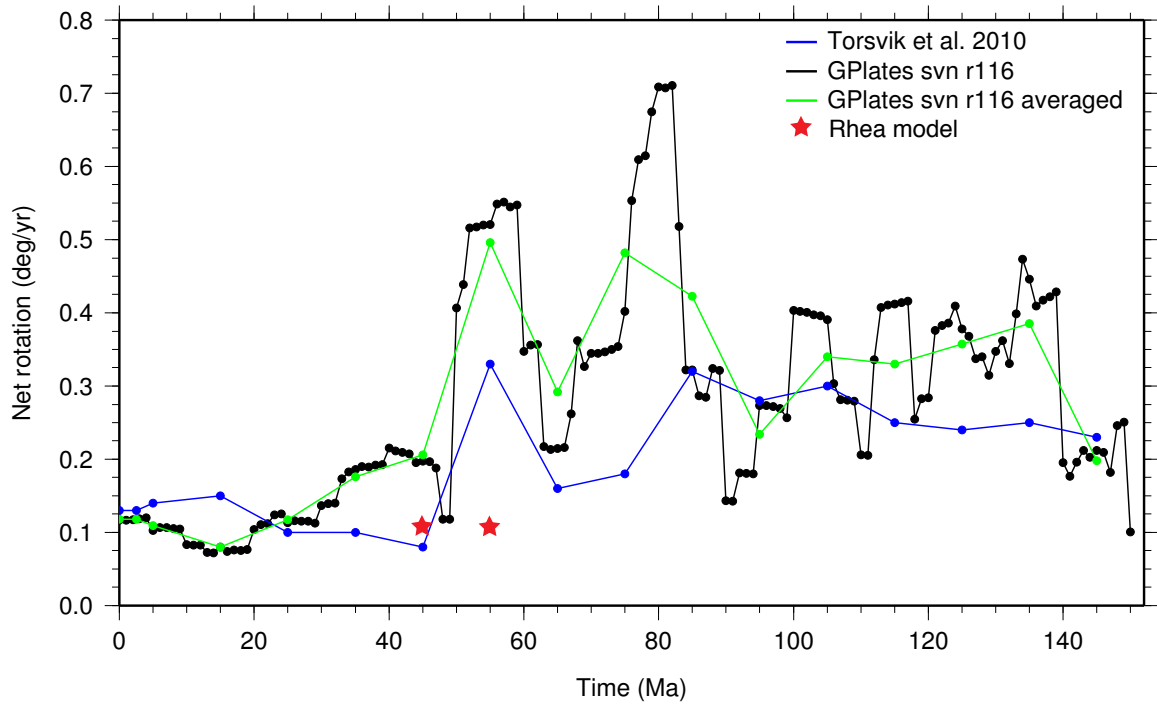


Figure 4.6. Time evolution of global net surface rotation. Blue: Prediction by *Torsvik et al.* (2010). Black: *GPlates* reconstruction used in this chapter. Green: *GPlates* net rotation averaged in the same time intervals as used by *Torsvik et al.* (2010) for comparison. Red stars: net rotation resulting from the dynamic motion models.

### 4.4.3 Surface State of Stress

The state of stress at the surface in the western Pacific is complicated. An interesting feature is the rotation of stresses along the western boundary of the Pacific plate (Figure 4.7). At 55 Ma, there is strong tension in the subducting Pacific plate perpendicular to the trench at the southern end of the boundary with Eurasia, indicating that subduction is readily occurring there. Further toward the north along the same boundary, this is changing into compression perpendicular to the trench, denoting a stronger resistance to subduction. and a reduction in slab pull.

There are two areas with significant changes in the state of stress between 55 and 45 Ma: just east of the center of the study area where the Izu-Bonin-Marianas subduction zone initiated, and in the southeast corner where the Tonga-Kermadec subduction zone initiated. In both cases, the stress regime in the subducting plate near the new trench has changed from compressional or partly tensional to strongly tensional perpendicular to the trench. Plates that are now overriding are all in compression near these trenches.

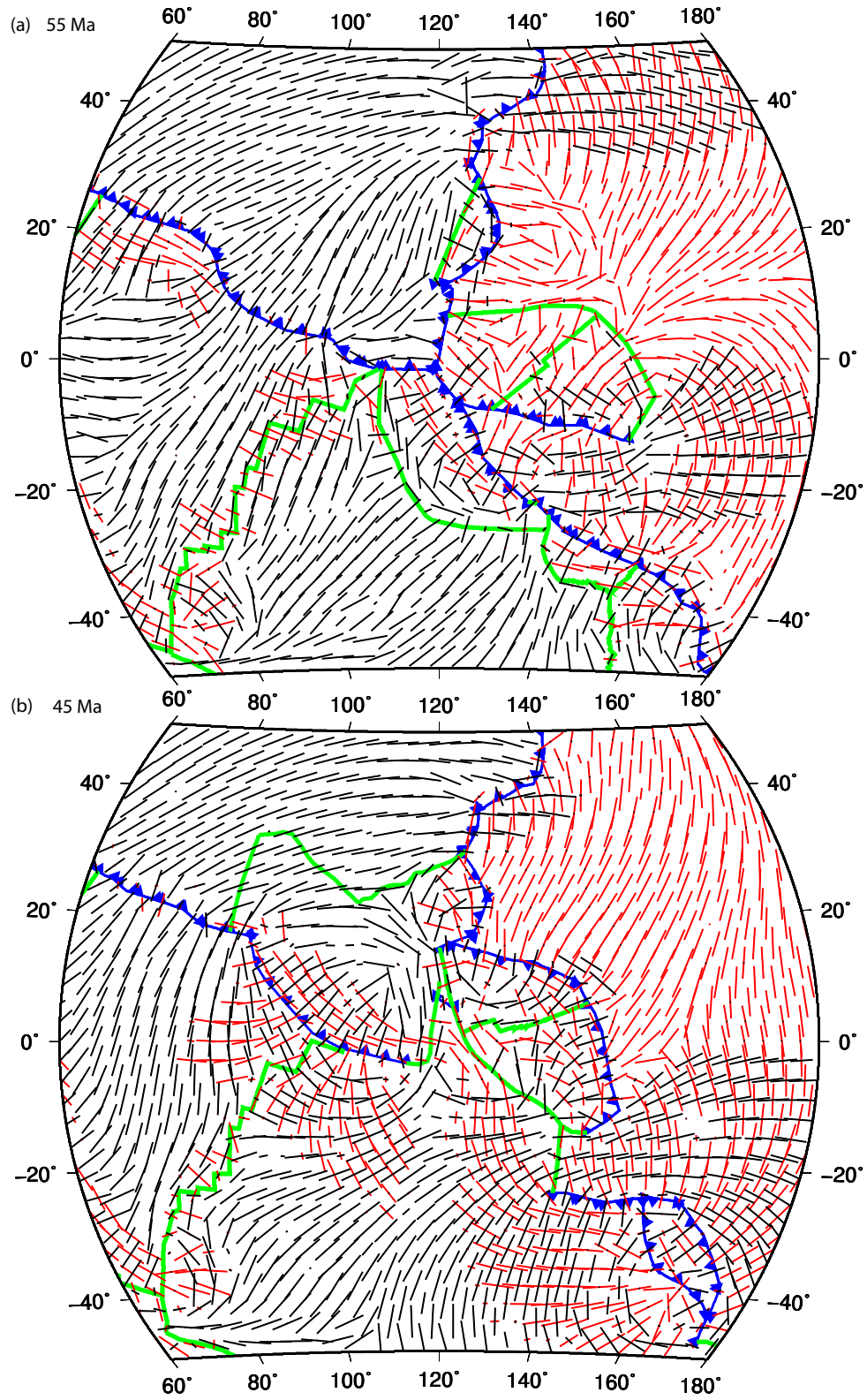


Figure 4.7. Map view of the surface state of stress, zoom-in on the western Pacific. (a) 55 Ma; (b) 45 Ma. Red dashes denote tension, black dashes show compression axes.

#### 4.4.4 Slabs

We now focus on the slabs in cross-sections around the Pacific Ocean: the Proto-South China Sea (PSCS) where the western Pacific subducts beneath Eurasia (Figures 4.8a–b and 4.9a–b); the Kuriles further to the north on the same boundary (Figures 4.8c–d and 4.9c–d); California, where the Farallon plate subducts underneath North America (Figures 4.8e–f and 4.9e–f); and Peru, where the Farallon plate subducts underneath South America (Figures 4.8g–h and 4.9g–h); see Figure 4.3a for the exact locations of the cross-sections.

In the Proto-South China Sea, the Pacific plate is subducted more or less perpendicular to the trench. Between  $\sim 300$  and  $660$  km depth, the slab has a reduced viscosity from  $10^{24}$  to  $\sim 10^{22}$  Pa s compared to the shallow slab, and has a lower velocity than its surroundings in this depth interval (Figure 4.8a). The loss of strength causes the motion of the lower mantle continuation of the slab to be slightly decoupled from the upper mantle slab. The majority of the slab is in compression, apart from the hinge (Figure 4.8b). The subducting Pacific plate is in tension, indicating that the slab is indeed pulling the Pacific plate down. At 45 Ma, the slab viscosity further decreases, and with it the coupling between the upper and lower mantle segments (Figure 4.9a). The shallow slab experiences more tension now (Figure 4.9b). The Kurile slab shows a similar decoupling between the upper and lower mantle slab at 55 Ma: the viscosity in the 300–660 km “gap” is only  $\sim 5 \times 10^{20}$  Pa s (Figure 4.8c). The Pacific plate is in compression and subducts slowly, since there is not much negative buoyancy attached to it to pull it down. The difference with the PSCS cross-section reflects the increase in resistance towards the north to subduction of the Pacific plate that was indicated by rotation of surface stresses. The upper mantle slab is in significant tension, transitioning to compression below 400 km depth (Figure 4.8d). The lower mantle is hardly moving, and does not appear to be coupled to the upper mantle flow. At 45 Ma, the upper mantle slab is even more decoupled

from the lower mantle high-viscosity structure, resulting in more significant tension (Figure 4.9c–d). The slab break-off at the East Asian subduction zone related to the arrival of the Izanagi-Pacific Ridge prior to 55 Ma resulted in slumping or avalanching of the slab remnant beneath the Pacific-Eurasia plate boundary, folding back on top of itself (visible in Figure 4.3b–c). This is illustrated by the tensional stress regime of the Pacific plate in the vicinity the East Asian subduction zone and in the still connected shallow slab.

On the other side of the Pacific ocean in California, there is more significant flow in the upper mantle around slabs. The Farallon slab is more strongly connected to the lower mantle compared to the western Pacific cross-sections (Figure 4.8e). The effect of lower mantle structure on dynamics is prominent: the velocities strongly decrease from the upper to the lower mantle as well as in the broad high-viscosity section of the slab just above the transition zone. In this case, the sharply defined and highly viscous lower mantle slab remnants inhibit the subducting slab motion, which is also indicated by the strong compressional regime throughout the entire slab (aside from its hinge which is in tension; see Figure 4.8f). The high-viscosity core of the slab extends deeper at 45 Ma, such that compression is even more dominant in the slab (Figure 4.9e–f). The slab in the Peru cross-section shows different behavior. The flow between upper and lower mantle is fully coupled at both 55 and 45 Ma, with a slab that has a high-viscosity core from the surface to the lower mantle (Figures 4.8g and 4.9g). This results in tension throughout the entire slab, as it is able to efficiently pull down the subducting plate (Figures 4.8h and 4.9h).

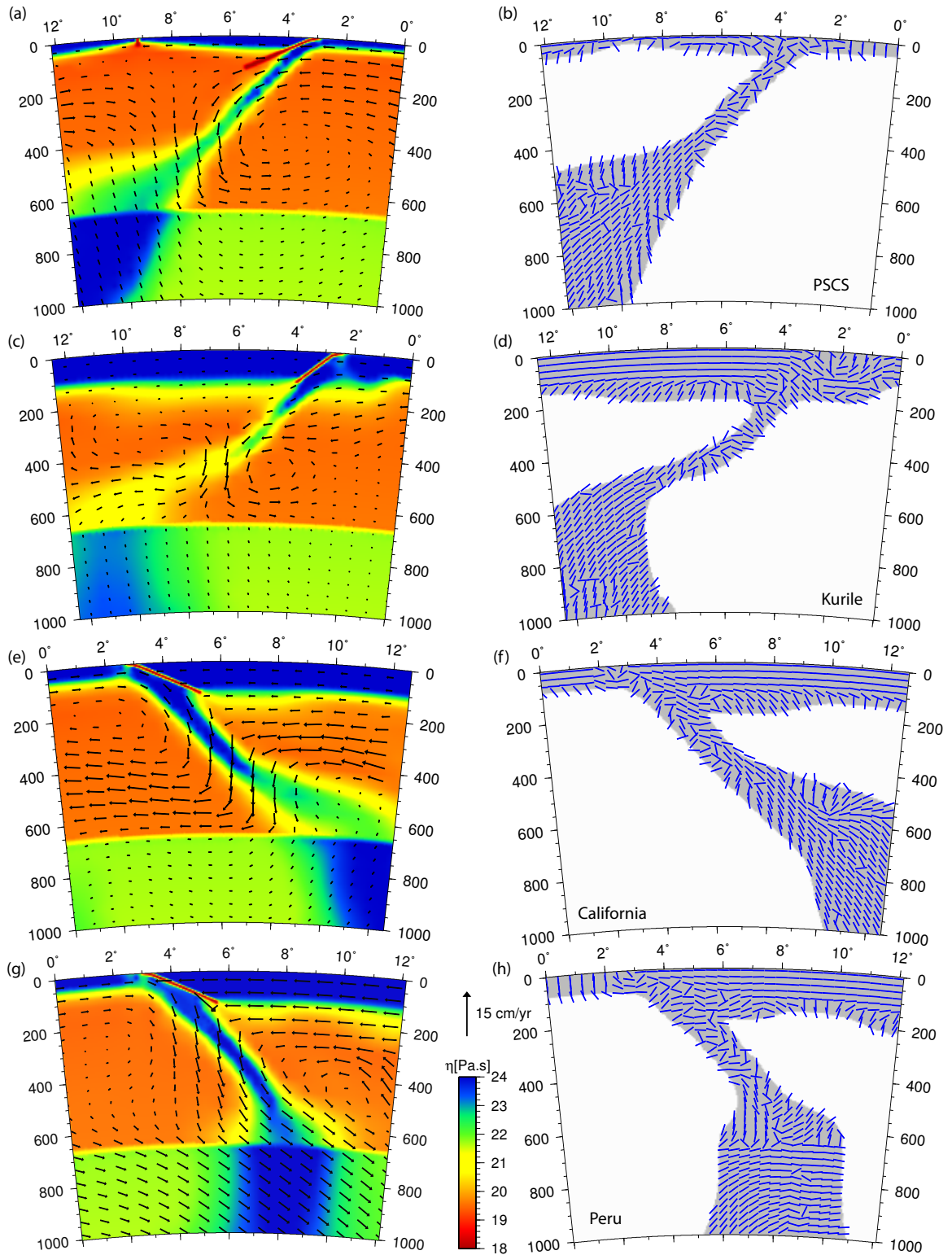


Figure 4.8. Cross-sections through subducting slabs at 55 Ma. Left column: viscosity and velocity. Right column: compression axes of unit length, with the grey background denoting the area with  $T < 0.9$ . (a)–(b): Proto-South China Sea (PSCS); (c)–(d) Kurile; (e)–(f) California; (g)–(h) Peru. See Figure 4.3a for the cross-section locations.

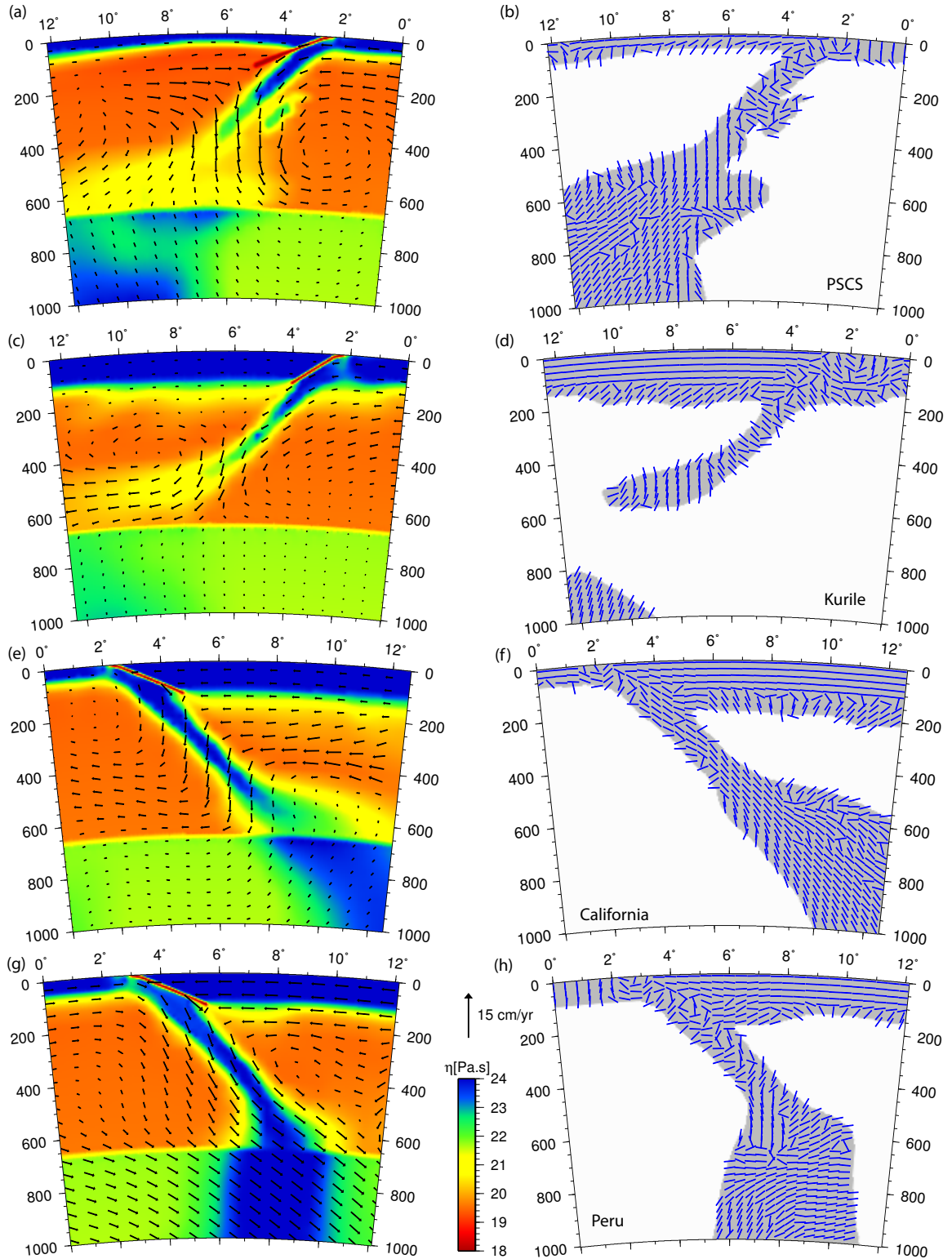


Figure 4.9. Cross-sections through subducting slabs at 45 Ma. Left column: viscosity and velocity. Right column: compression axes of unit length, with the grey background denoting the area with  $T < 0.9$ . (a)–(b): Proto-South China Sea (PSCS); (c)–(d) Kurile; (e)–(f) California; (g)–(h) Peru. See Figure 4.3a for the cross-section locations.

Overall, several patterns emerge. Plates only efficiently subduct when the upper mantle slabs are sufficiently connected to their lower mantle counterparts. This effect, or the lack of it, becomes evident in the northwestern Pacific (Figure 4.10): the high viscosity segments at 700 km depth in that area do not correspond to slabs outlined by low temperature at 600 km depth. This missing pull could be a cause for the misfit of the Pacific plate motion, which moves too much to the west without the predicted significant northerly component. In contrast, a strong overlap of the slab outline at 600 km depth and high-viscosity structures at 700 km depth in Central and South America corresponds to strongly coupled slabs. This difference in behavior between the western Pacific and the Americas can be attributed to the age of the plate subducted in the preceding period. In the PSCS and Kurile area, the young Izanagi plate and the Izanagi-Pacific Ridge were just subducted, leading to a thin slab with limited coupling. The Farallon plate subducted beneath California and especially under Peru was significantly older, resulting in thick and strongly coupled slabs, with connected lower mantle structures that dip almost vertically into the mantle. An even more extreme example can be seen in southern Eurasia, where the very old and thick African plate is subducting, resulting in strongly connected slabs.

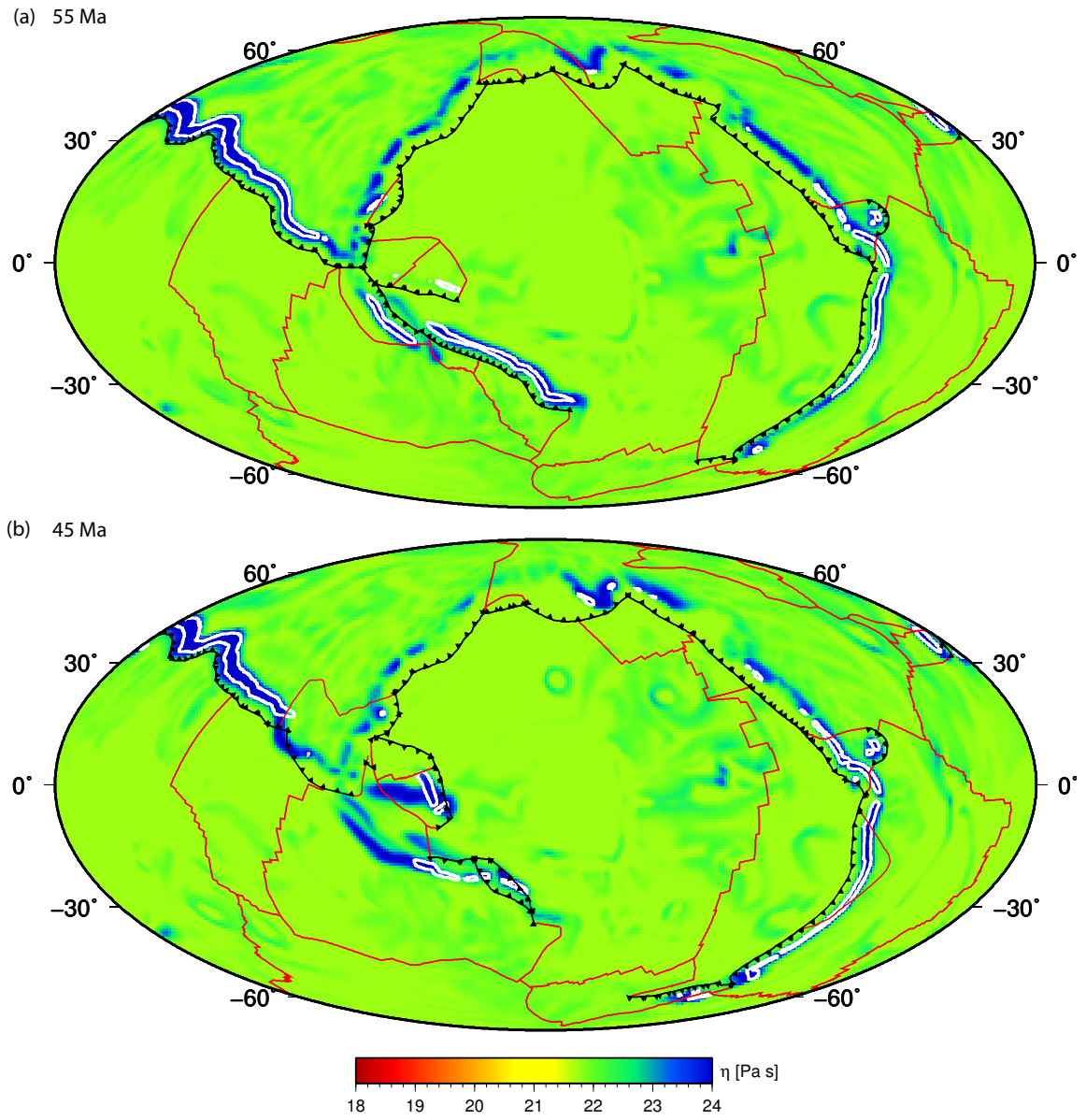


Figure 4.10. Viscosity field at 700 km depth (color map), with slab contours at 600 km depth plotted in white contours. The contours are defined by the nondimensional temperature  $T = 0.8$ .

#### 4.4.5 Lateral Mantle Flow

The stationary upwelling under the central Pacific, corresponding to the Hawaiian hotspot location, dominates the sub-Pacific flow pattern (Figure 4.11). Flow beneath continents appears irregular, being dominated by small-scale drips from the lithosphere that have a higher viscosity compared to the ambient mantle. These features may decrease the ability of the continental lithosphere to decouple from the upper mantle, and hence they slow continental plate motion.

The presence of slabs affects lateral flow in the mantle. The pattern in the western Pacific shows that trench-perpendicular flow is dominant. Especially at 400 km depth, the largest lateral flow occurs through gaps in the subducting Pacific slab, where the flow is funneled and accelerated. The initiation of the Izu-Bonin-Marianas and Tonga-Kermadec subduction prior to 45 Ma causes the flow pattern at 45 Ma to locally diverge from that at 55 Ma. However, the overall pattern at 400 km depth is not significantly altered, and differences at 800 km depth are more or less indiscernable. This implies that it is unlikely that general sub-Pacific mantle flow could be altered or slowed by the subduction of slabs in the IBM and TK subduction zones, as was suggested by *Whittaker et al.* (2007). Instead, changes in flow patterns are highly localized, likely due to the nonlinear rheology. In areas where flow is enhanced such as around slabs, the high strain rate will lower the viscosity, which further increases velocities but also limits the extent of the area affected by the presence of the slab.

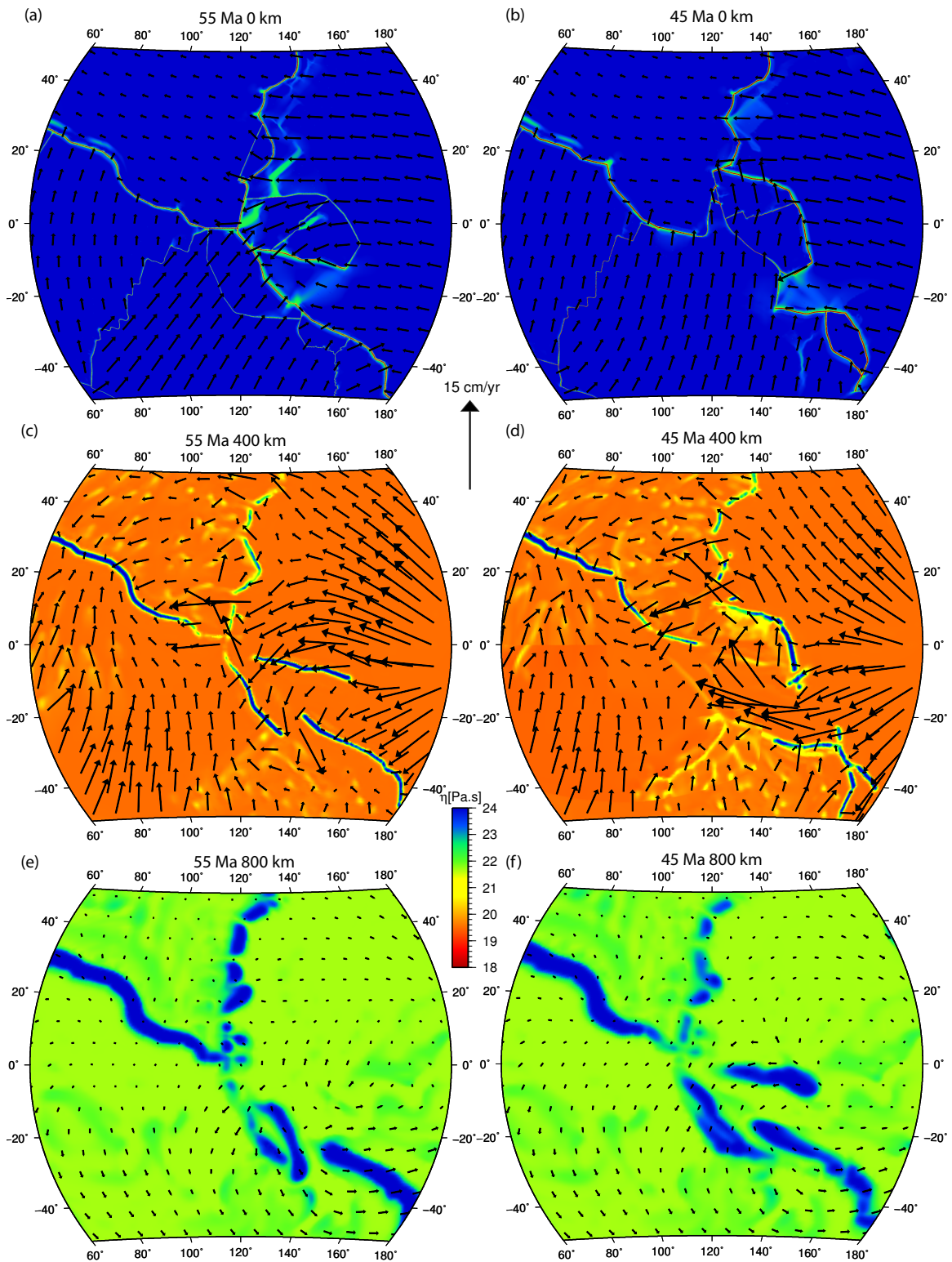


Figure 4.11. Map view of lateral mantle flow plotted on viscosity, zoom-in on western Pacific; 55 Ma (left) and 45 Ma (right). (a)–(b): Surface; (c)–(d): 400 km depth; (e)–(f): 800 km depth.

## 4.5 Discussion

Despite the implementation of a nonlinear rheology and detailed reconstructed plate boundaries, lithospheric thickness, and assimilated slabs with their appropriate age, plate motions only change slowly between 55 and 45 Ma, which results in a poor fit of plate motions in the dynamic convection models to predictions from paleo plate reconstructions. We are therefore currently not able to reproduce the rapid plate reorganizations.

Several important model aspects have come to light. A major difference with the present-day models of Chapter 3 is the nature of the lower mantle viscosity. The tomography used for the present-day models results in smooth, broad high-viscosity features. In contrast, advected slabs in a convection model remain much sharper with higher viscosities. Depending on the morphology of the slab remnants, these sharply defined features in the lower mantle can add significant slab pull to the subducting plate when they are narrow and steeply dipping, such as beneath Peru. They can also act as brakes on subduction when the slab has folded back onto itself, forming an anchor in the lower mantle, much like the broad features in the present-day models. This suggests that the details of the lower mantle structure, and therefore parameter choices in the time-dependent models, strongly affect outcomes of these instantaneous models. In the models presented here, the lower mantle structures dominate the model dynamics, such that relatively small changes in plate boundary configurations do not significantly affect plate motions. Similarly, these stationary features anchor the overall flow, including the plates, allowing little motion of the surface with respect to the lower mantle (i.e., a small net rotation).

The amount of coupling within slabs and between slabs and plates is directly affected by the age and therefore the thickness of the subducted slab: older, thicker slabs such as the

Farallon slab connect lower mantle structure to plates more strongly than younger, thinner ones such as Izanagi. The coupling of slabs with the surrounding mantle depends on slab morphology and the ambient viscosity: in the upper mantle with a relatively low viscosity, the flow affected by thin slabs is limited in its spatial extent. This implies that the descending slabs in the Izu-Bonin-Marianas and Tonga-Kermadec subduction zones are not likely to be responsible for the slowdown of the sub-Pacific mantle, as was suggested by *Whittaker et al.* (2007).

We do not observe the extension of the overriding plate following initiation of the IBM subduction zone that was predicted by *Hall et al.* (2003) to explain inferred catastrophic boninitic volcanism associated with the subduction initiation. This extension in the overriding plate is however not expected to be seen in global dynamic models, as these regional models are time dependent and there is a strong feedback between the slab and development of spreading on the overriding plate.

Potential improvements to the instantaneous dynamic models could be made by using time dependent models for the mantle structure that have fewer slab remnants in the lower mantle. If a plate model instead of a half-space cooling model is used such that the subducting slab age is truncated at 80 Ma (see, e.g., *Steinberger and Torsvik* (2010)), slab thickness and therefore the lifespan of slabs in the lower mantle would be reduced. This would promote overall flow in the mantle, and could possibly increase the ability of slabs to subduct into the lower mantle more easily. In addition, the higher-viscosity lithospheric drips underneath the continents possibly add resistance to motion of the plates in the form of basal drag; their removal by, e.g., implementing a more realistic continental age distribution could enhance overall plate speeds and fit to predicted plate motions. Furthermore, it would be instructive to compute a dynamic model prior to the slab break-off at the East Asia subduction zone (at, e.g., 65 Ma), such that

the effect of the presence of slabs and slab break-off on global plate motions and state of stress can be studied more closely. Another interesting topic for further investigation is the evolution of the net surface rotation and its discrepancy between the dynamic plate motion models, the plate reconstruction model, and the reconstructions by *Torsvik et al.* (2010).

## 4.6 Conclusions

We computed high-resolution dynamic global convection models at 55 and 45 Ma in order to study the plate reorganization taking place around 50 Ma. These instantaneous models are constructed using the result of lower-resolution time-dependent models to populate mantle structure. Slab remnants in the lower mantle are abundant and sharply defined with high viscosities, and strongly influence plate motions and flow in the mantle interior. While modeled plate motions do not show a good fit to reconstructed plate motions, it has become apparent that slab age is an important factor in slab pull, through coupling between plates and slabs and between upper and lower mantle sections of slabs. We further find that subducting slabs are not capable of affecting lateral flow in the upper mantle on a large scale, and therefore we conclude that it is unlikely that the slabs in the western Pacific are responsible for the slowing of sub-Pacific flow after the initiation of their subduction.

## Acknowledgements

We would like to thank Kara Matthews for her work on the `GPlates` plate reconstructions resulting in the plate boundary weak zones, Maria Seton for the age grid reconstructions, and Dan Bower and Nico Flament for making their `CitcomS` convection models available. Discussions with Dietmar Müller and Trond Torsvik were also highly beneficial. This work

was partially supported by the NSF PetaApps program (OCI-0749334, OCI-0748898), NSF Earth Sciences (EAR-0426271, EAR-0810303), and the Caltech Tectonics Observatory (by the Gordon and Betty Moore Foundation). Computing resources on TACC Lonestar and Spur systems were provided through the NSF TeraGrid under grant number TG-MCA04N026. The figures were produced using Generic Mapping Tools (GMT) and Paraview.